Electroweak physics at the LHC

J Berryhill[1] and A Oh[2]

[1] Fermi National Accelerator Laboratory, Batavia, IL, USA

[2] School of Physics and Astronomy, University of Manchester, Manchester, UK

Abstract. The Large Hadron Collider (LHC) has completed in 2012 its first running phase and the experiments have collected data sets of pp collisions at center-of-mass energies of 7 and 8 TeV with an integrated luminosity of about 5 $fb^{-1}$and 20 fb^{-1}, respectively. Analyses of these data sets have produced a rich set of results in the electroweak sector of the standard model. This article reviews the status of electroweak measurements of the ATLAS and CMS experiments at the LHC and discusses phenomenological developments in the electroweak sector.

PACS numbers: 12.15.-y, 12.60.Cn, 14.70.-e

Submitted to: *J. Phys. G: Nucl. Part. Phys.*

At a hadron collider, the most fundamental tests of electroweak boson couplings to fermions are measurements of the kinematic properties of Drell-Yan (DY) lepton pair production. At leading order, Drell-Yan production occurs when a quark–anti-quark pair in the intial state annihilates into an electroweak boson, which subsequently decays to a lepton pair. Differential cross section calculations exist for next-to-next-to leading order (NNLO) QCD corrections as well as NLO electroweak corrections. In the EFT context, such a process is sensitive to four-fermion contact interactions of the type

$$\begin{aligned}\mathcal{L} = \tfrac{g^2}{\Lambda^2}\,[\quad & \eta_{\rm LL}\ (\overline{q}_{\rm L}\gamma_\mu q_{\rm L})\,(\overline{\ell}_{\rm L}\gamma^\mu \ell_{\rm L}) \\ & +\eta_{\rm RR}\,(\overline{q}_{\rm R}\gamma_\mu q_{\rm R})\,(\overline{\ell}_{\rm R}\gamma^\mu \ell_{\rm R}) \\ & +\eta_{\rm LR}\,(\overline{q}_{\rm L}\gamma_\mu q_{\rm L})\,(\overline{\ell}_{\rm R}\gamma^\mu \ell_{\rm R}) \\ & +\eta_{\rm RL}\,(\overline{q}_{\rm R}\gamma_\mu q_{\rm R})\,(\overline{\ell}_{\rm L}\gamma^\mu \ell_{\rm L})\ ]\,,\end{aligned} \tag{1}$$

where g is a coupling constant, Λ is the contact interaction scale, and $q_{\rm L,R}$ and $\ell_{\rm L,R}$ are left-handed and right-handed quark and lepton fields, respectively. The parameters $\eta_{i,j}$ denote the relative interference of the operators; the experiments have considered the cases $\eta_{\rm LR} = \eta_{\rm RL} = \pm 1$, $\eta_{\rm LL} = \pm 1$, or $\eta_{\rm RR} = \pm 1$.

Experiments select electron or muon pairs above trigger thresholds: CMS selects leading lepton $p_T > 17$ GeV and second leading lepton $p_T > 8$ GeV inclusively, and ATLAS selects high mass events with both lepton $p_T > 25$ GeV. Backgrounds to Drell-Yan production are relatively small, and consist of real prompt lepton pair production from top quark or boson pairs, as well as fake electrons from QCD jets. The real lepton pair background is flavor democratic, and can therefore be reliably estimated from $e\mu$ pair production. Fake electron production is typically estimated from background enriched QCD jet samples, from which the fake electron rate can be measured, convolved with electron-jet control samples.

Figure 1 shows the Drell-Yan cross section at high electron pair mass measured by ATLAS at 7 TeV [1]. The cross section uncertainty is predominantly systematic below 400 GeV in pair mass and predominantly statistical above 400 GeV. The data are compared with an NNLO QCD prediction with NLO electroweak corrections, provided by the FEWZ 3.1 generator [**?**]. The prediction also includes photon induced lepton pair production, which generally increases cross section estimates by a few percent. The FEWZ prediction generally underestimates the cross section, however a correlated chi-squared analysis concludes that this is not statistically significant.

Figure 2 shows the Drell-Yan cross section for electron or muon pairs measured by CMS at 8 TeV [2]. Agreement with the FEWZ prediction is observed over the entire measured mass range, from 15 GeV to 2000 GeV. CMS has also measured the double differential cross section with respect to dilepton rapidity in several bins of dilepton mass, as well as a differential cross section ratio between the 8 TeV and 7 TeV data, which has small experimental and theoretical uncertainties.

In the absence of observed disagreements with predictions at the highest dilepton masses, the data are analyzed to constrain the size of anomalous contact interactions. Assuming a fixed, strong value for the coupling ($g^2/4\pi = 1$), limits can be obtained

on the contact interaction scale Λ. ATLAS estimates a lower limit of 17 to 26 TeV on Λ, where the strongest lower limits correspond to constructive interference scenarios (especially LR+RL), and the weakest to destructive interference scenarios [**?**]. CMS has limits with similar sensitivity estimated for LL contact interactions [**?**].

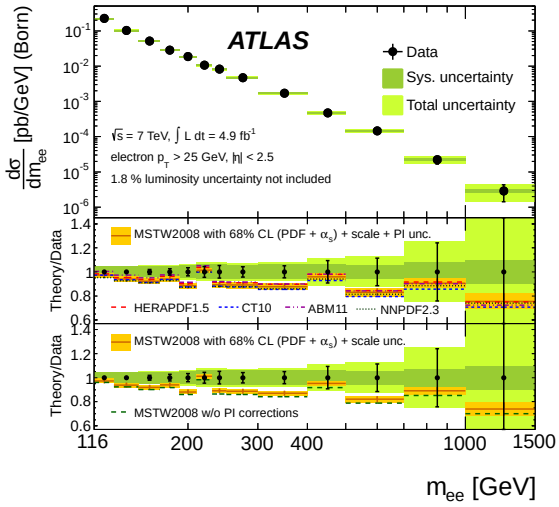

Figure 1. Measured differential cross-section at the Born level within the fiducial region (electron $p_{\mathrm{T}} > 25$ GeV and $|\eta| < 2.5$) with statistical, systematic, and combined statistical and systematic (total) uncertainties, excluding the 1.8% uncertainty on the luminosity. On the left, in the upper ratio plot, the photon-induced (PI) corrections have been added to the predictions obtained from the MSTW2008, HERAPDF1.5, CT10, ABM11 and NNPDF2.3 NNLO PDFs, and for the MSTW2008 prediction the total uncertainty band arising from the PDF, α_s, renormalisation and factorisation scale, and photon-induced uncertainties is drawn. The lower ratio plot shows the influence of the photon-induced corrections on the MSTW2008 prediction, the uncertainty band including only the PDF, α_s and scale uncertainties.

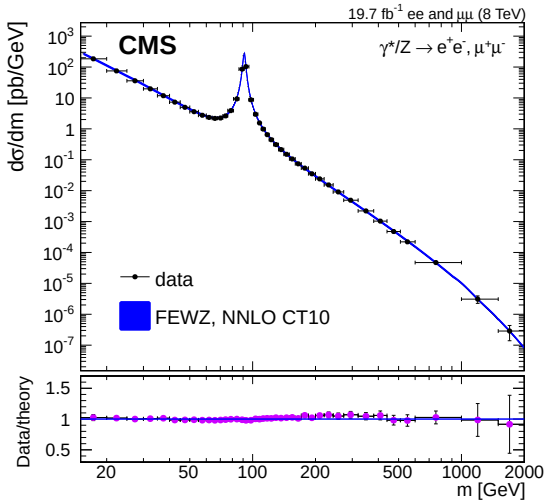

Figure 2. The DY differential cross section as measured in the combined dilepton channel and as predicted by NNLO FEWZ 3.1 with CT10 PDF calculations, for the full phase space.

3.2. Inclusive di-boson production

ATLAS $W^{\pm}\gamma$ $Z\gamma$ 7 TeV [3]
CMS $W^{\pm}\gamma/Z\gamma$ 7 TeV [4]
CMS $Z(\nu\bar{\nu})\gamma$ 7 TeV [5]
CMS $Z\gamma$ 8 TeV [6]
ATLAS simultaneous tt/WW/Z cross section 7 TeV [7]
ATLAS WW 7 TeV [8]
ATLAS WW+WZ cross section 7 TeV [9]
ATLAS WW 8 TeV [10]
CMS WW2l2n 7 TeV [11]
CMS WWlnjj 7 TeV [12]
CMS WW/ZZ 8 TeV [13]
CMS WW2l2n 8 TeV(CMS-PAS-SMP-14-016, to be published)
ATLAS WZ 7 TeV [14]
CMS VZ 8 TeV [15]
CMS WZ at 7+8 TeV(CMS-PAS-SMP-12-006, to be published)

3.2.1. ZZ production The production of ZZ in proton-proton collisions has been one of the first di-boson processes measured at the LHC. The SM process is and an important and irreducible background to resonance searches and Higgs production. The production at leading order is dominated by quark anti-quark annihilation in the t and u-channel, whereas the s-channel process is forbidden in the SM (see also Figure 3). The gluon fusion process contributes about 6% to the total production cross section.

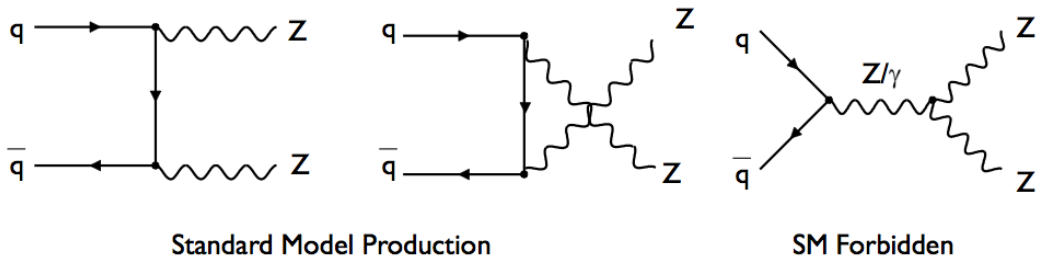

Figure 3. Leading order Feynman diagrams of ZZ production in the dominant $q\bar{q}$ channel. The ZZ production via the s-channel is not allowed in the SM.

Precision measurements use the leptonic decay modes of the Z to reduce the impact of QCD backgrounds. The four lepton final state provides an almost background free signature, at the expense of a relatively small branching ratio $BR(ZZ) \rightarrow \ell^+\ell^-\ell^+\ell^- = 0.101^2 \cdot \frac{4}{9} = 0.0045$ [**?**]. The di-lepton and missing energy channel can exploit the one order of magnitude higher branching ratio of $BR(ZZ \rightarrow \ell^+\ell^-\nu\bar{\nu}) = 0.101 \cdot 0.20 \cdot 2 \cdot \frac{2}{3} = 0.0269$, at the expense of high background levels.

The ATLAS collaboration has published results on the 7 TeV data-set in the $\ell^+\ell^-\ell^+\ell^-$ and $\ell^+\ell^-\nu\bar{\nu}$ final state [16]. The CMS collaboration has analysed the full 7 and 8 TeV data sets in both the $\ell^+\ell^-\ell^+\ell^-$ [17, **?**] and $\ell^+\ell^-\nu\bar{\nu}$ final state [18].

Theoretical predictions for ZZ production are available at NLO in α_s [**?**]. In addition, electroweak corrections at NLO have been calculated [**?**, **?**].

The event selection for the $\ell^+\ell^-\ell^+\ell^-$ final state requires exactly four leptons fulfilling a set of cuts on kinematic quantities. ATLAS and CMS use similar criteria as listed in detail in Table **??**. While ATLAS uses $l = e, \mu$, CMS includes also $Z \rightarrow \tau^+\tau^-$ with subsequent hadronic and leptonic τ decays. ATLAS uses in addition forward leptons outside the ID tracker to increase the acceptance by 6% for electrons and 10% for muons. The $\ell^+\ell^-\ell^+\ell^-$ channels offers the cleanest event sample with a background level of only $2-3\%$ from $Z + jets$, , and di-boson events. The background is estimated from data by control regions with looser selection criteria.

Events in the $\ell^+\ell^-\nu\bar{\nu}$ final state are characterized by exactly two leptons and missing energy. The event selection requires a leptonic Z candidate and missing energy in the event. Both experiments used refined observables of missing energy with additional information to improve the rejection against instrumental background. The background level is in the same order as the signal and substantially higher then for $\ell^+\ell^-\ell^+\ell^-$. Main background sources are $V + jets$, and di-boson production. ATLAS and CMS

use data driven techniques to constrain the dominant background sources.

Besides the total cross section for the $pp \to ZZ$ production process, both experiments measure also fiducial and differential cross sections. The results are summarized in Tabel 1. ATLAS and CMS use different definitions of the fiducial phase space which needs to be taken into account to make a direct comparison is possible. For the total cross section a slightly different mass range for the Z mass range is used, where CMS uses a wider range of 60 GeV $< m_Z <$ 120 GeV then ATLAS with 76 GeV $< m_Z <$ 116 GeV, which contributes to the difference in the quoted predicted cross section. Agreement of experimental and theoretical cross section values is observed.

Experiment	decay channel	$\sqrt{s}$	measured σ_{total} [pb]	predicted σ_{total} [pb]	reference
ATLAS	$\ell^+\ell^-\ell^+\ell^-$, $\ell^+\ell^-\nu\bar{\nu}$	7 TeV	6.7 $\pm$ 0.7 (stat.) $^{+0.4}_{-0.3}$ (syst.) $\pm$ 0.3 (lumi.)	$6.18^{+0.25}_{-0.18}$	[16]
CMS	$\ell^+\ell^-\ell^+\ell^-$	7 TeV	6.2 $\pm$ $^{+0.9}_{-0.8}$ (stat.) $^{+0.4}_{-0.3}$ (syst.) $\pm$ 0.1 (lumi.)	6.3$\pm$0.4	[17]
CMS	$\ell^+\ell^-\nu\bar{\nu}$	7 TeV	5.2 $\pm$ $^{+1.5}_{-1.4}$ (stat.) $^{+1.4}_{-1.1}$ (syst.) $\pm$ 0.2 (lumi.)	6.1$\pm$0.3	[17]
CMS	$\ell^+\ell^-\ell^+\ell^-$	8 TeV	7.7 $\pm$ 0.5 (stat.) $^{+0.5}_{-0.4}$ (syst.) $\pm$ 0.2 (lumi.)	7.7$\pm$0.6	[19]
CMS	$\ell^+\ell^-\nu\bar{\nu}$	8 TeV	6.9 $\pm$ 0.8 (stat.) $^{+1.8}_{-1.4}$ (syst.) $\pm$ 0.3 (lumi.)	7.6$\pm$0.3	[17]

Table 1. Summary of measured ZZ production cross sections from ATLAS and CMS at 7 and 8 TeV centre-of-mass energies in the four lepton and $\ell^+\ell^-\nu\bar{\nu}$ final state.

Limits on ATGC parameters are determined with differential distributions of the invariant di-boson mass (CMS, four lepton channel), the transverse momentum of the leading lepton (CMS, $\ell^+\ell^-\nu\bar{\nu}$-channel), or the transverse momentum of the leading Z(ATLAS, all channels). A comparison of the measured and predicted differential cross sections in the four-lepton invariant mass is shown from CMS in Figure 4. Also shown is the prediction in the presence of a non-zero value of the anomalous coupling parameter $f_4^Z = 0.015$, which shows an enhancement over the SM value at high invariant masses.

Both experiment publish 95% CL limits on ATGC without form factors in the $\ell^+\ell^-\ell^+\ell^-$ and $\ell^+\ell^-\nu\bar{\nu}$ channels. The results are in agreement with the SM and summarized in Figure 5 taken from Ref. [20]. The precision of the LHC results is driven by the steep increase of sensitivity with higher centre-of-mass energy and are about 2 orders of magnitude better compared to the combined LEP result [21].

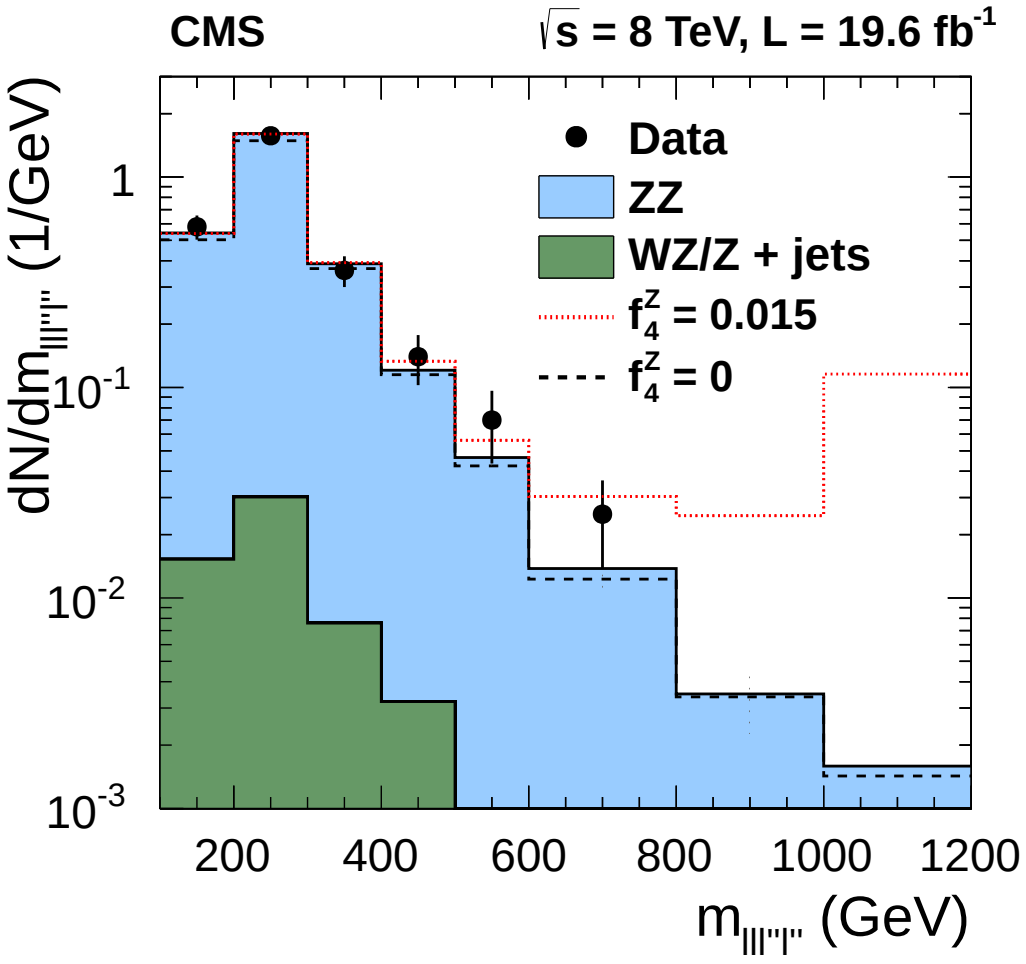

Figure 4. Distribution of the four-lepton reconstructed mass for the combined $4e$, 4μ, and $2e2\mu$ channels from CMS [**?**]. Points represent the data, the shaded histogram labeled ZZ represents the predictions for ZZ signal, the histograms labeled $W^{\pm}Z/Z$+jets shows background estimated form data. The dashed and dotted histograms indicate the SM expectation (f4Z = 0) and in the presence of an ATGC (f4Z = 0.015) with all the other anomalous couplings set to zero. The last bin includes all entries with masses above 1000 GeV.

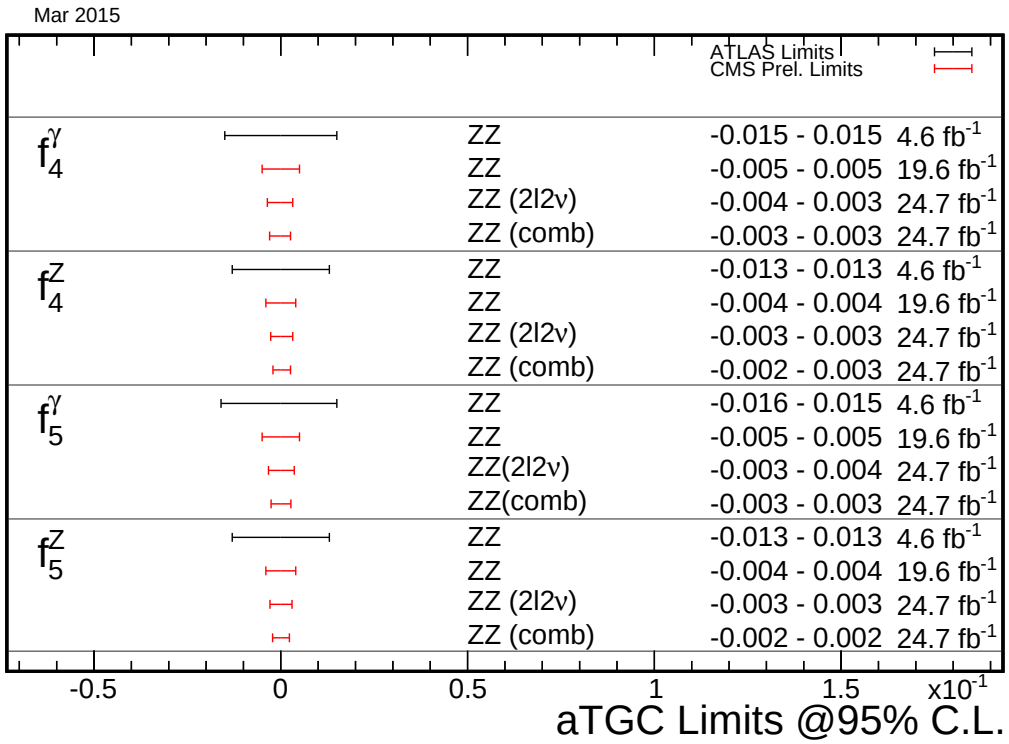

Figure 5. Comparison of the limits on f_{40}^V and f_{50}^V from ATLAS and CMS in the $\ell^+\ell^-\ell^+\ell^-$ and $\ell^+\ell^-\nu\bar{\nu}$ channel at 7 and 8 TeV.

3.2.2. WZ production At the LHC, $W^{\pm}Z$ diboson are produced from quark-antiquark initial states at leading order (LO) and quark-gluon initial states at next-to-leading order (NLO) [**?**]. The SM allowed s-channel diagram has a triple boson vertex and is sensitive to anomalous TGC of gauge bosons.

The ATLAS experiment measured the $W^{\pm}Z$ production cross section in the fully leptonic decay channel $\ell^+\ell^-\ell\nu$ [14] at $\sqrt{s} = 7$ TeV and set limits on anomalous charged TGC. In this analysis the final states involving electrons or muons are considered signal, whereas boson decays to tau's are considered as background. The dominant background sources are Z+jet and ZZ production, constituting about 40% of the background. The overall signal over background ratio is about 3.7. The dominant systematic uncertainty is from the data-driven estimate of the background, where the dominant Z + jets contributes with ($\pm 3.8\%$).

The fiducial cross section defined by $p_{\mathrm{T}}^{\mu,e} > 15$ GeV for the leptons from the Z decay, $p_{\mathrm{T}}^{\mu,e} > 15$ GeV for the lepton from the W, $|\eta^{\mu,e}| < 2.5$, $p_{\mathrm{T}}^{\nu} > 25$ GeV, $|m_l l - m_Z| < 10$ GeV, $M_T^W > 20GeV$ and $\Delta R > 0.3$ for the three possible $\ell\ell$ pairings. The fiducial and total cross sections are compared to the SM expectation at NLO in Table 3.2.2.

Experiment	cross section	$\sqrt{s}$	measured	predicted	reference
ATLAS	total	7 GeV	$19^{+1.4}_{-1.3}$ (stat.) ± 0.9 (syst.) $\pm$ 0.4 (lumi.) pb	$17.6 \pm {}^{+1.1}_{-1.0}$ pb	[14]
ATLAS	fiducial	7 GeV	$92 \pm {}^{+7}_{-6}$ (stat.) ± 4 (syst.) $\pm$ 2 (lumi.) fb	–	[14]

Table 2. Summary of measured fiducial and total $W^{\pm}Z$ production cross sections from ATLAS at 7 TeV centre-of-mass energies in the $\ell^+\ell^-\ell\nu$ final state.

In Figure 7 the differential cross section measured in bins of p_{T}^Z is shown, compared to SM prediction and a set of anomalous TGC couplings. The normalized p_{T}^Z spectrum is unfolded and compared to the NLO calculation of MC@NLO in Figure 7, showing good agreement with the SM.

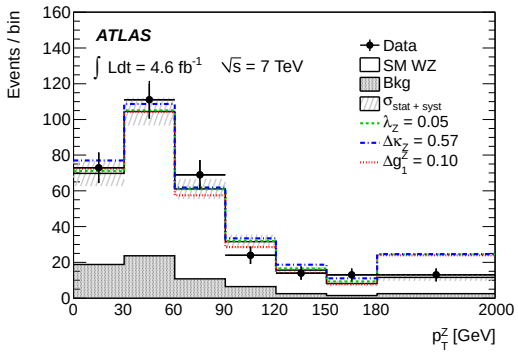

Figure 6. ATLAS measurement of the transverse momentum of the Zin $W^{\pm}Z$ events (p_{T}^Z) compared with the SM prediction at $\sqrt{s} = 7$ TeV. For illustration calculations for a set of anomalous couplings values are also shown. The full uncertainty contains statistical and systematic uncertainties.

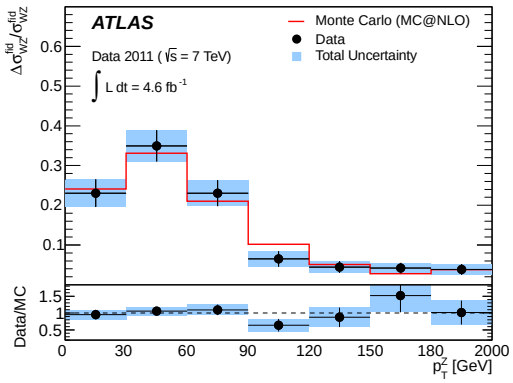

Figure 7. ATLAS measurement of the normalized fiducial cross-sections in bins of p_{T}^{Z} compared with the SM prediction at $\sqrt{s} = 7$ TeV. The full uncertainty contains statistical and systematic uncertainties.

Table 3. Expected and observed 95% CL on $\Delta\kappa_Z$, λ_Z and g_1^Z.

	Observed $\Lambda = 2$ TeV	Observed no form factor	Expected no form factor
g_1^Z	$[-0.074, 0.133]$	$[-0.057, 0.093]$	$[-0.046, 0.080]$
$\Delta\kappa_Z$	$[-0.42, 0.69]$	$[-0.37, 0.57]$	$[-0.33, 0.47]$
λ_Z	$[-0.064, 0.066]$	$[-0.046, 0.047]$	$[-0.041, 0.040]$

Limits on the charged ATGC parameters $\Delta\kappa_Z$, λ_Z and g_1^Z are extracted from the transverse momentum distribution of the Z, p_{T}^{Z}. The ATGC parameter 95% CL limits are quoted using a form-factor of $\Lambda = 2$ TeV and without a form-factor, and summarized in Table 5.

3.2.3. WW production The W^+W^- production process has the highest production cross section among the massive vector diboson processes. It is also an important background process to Higgs production and to searches for new physics. ATLAS and CMS, observed the W^+W^- production process in the fully leptonic channel and published results for 7 TeV (ATLAS [8],CMS [11]) and 8 TeV (CMS [13]) centre-of-mass energy. Three final states, namely ee, $\mu\mu$, and $e\mu$ are included in the analyses. The contribution from leptonically decaying τ leptons is included in the signal definition. Although the production cross section is relatively high, the signature of two opposite sign leptons and missing transverse energy is shared with many processes and a careful control of the backgrounds is necessary to achieve a precise measurement.

Candidate W^+W^- events are selected by by requiring two oppositely charged leptons accompanied with large $E_{\mathrm{T}}^{\mathrm{miss}}$. The dominant background sources are $t\bar{t}$ and single top quark, $W^{\pm}$/+jets, followed by Z/γ^*+jets production. To suppress the dominant $t\bar{t}$ background, events with one or more jets are rejected. Additional requirements on $E_{\mathrm{T}}^{\mathrm{miss}}$ and the use of top quark-taggers further reduce the residual background to about 30%. The dominant systematic uncertainty is related to the jet veto efficiency and estimated to about 5% for the W^+W^- production. The experiments quote a theoretical uncertainties on the signal acceptance due to variations of the parton distribution functions and renormalisation and factorization scale in the range of 1-2%.

Both ATLAS and CMS provide a measurement of the total cross section for the process $pp \to W^+W^-$ and compare to theoretical calculations. The Higgs process contributes with about 4% to the total cross section and has not been taken into account in the comparison to the SM predictions. The total cross section results are summarised in Table 3.2.3. A good agreement of the experiments for the measured cross section as well as for the theoretical predictions is observed. A normalised differential measurement of the fiducial cross section in bins of p_{T} of the leading lepton is presented by ATLAS, as shown in Figure 8. The unfolded spectrum is in agreement with the SM prediction. The

3.2.3.

Experiment	cross section	$\sqrt{s}$	measured	predicted	reference
ATLAS	total	7 GeV	51.9 ±2.0 (stat.) 3.9 (syst.) ± 2.0 (lumi.) pb	$44.7\ ^{+2.1}_{-1.9}$ pb	[8]
CMS	total	7 GeV	52.4 ±2.0 (stat.) 4.5 (syst.) ± 1.2 (lumi.) pb	47.0 ±2.0 pb	[11]
CMS	total	8 GeV	69.9 ±2.8 (stat.) 5.6 (syst.) ± 3.1 (lumi.) pb	$57.3\ ^{+2.3}_{-1.6}$ pb	[11]

Table 4. Summary of measured fiducial and total W^+W^- production cross sections from ATLAS and CMS at 7 and 8 TeV centre-of-mass energies in the $\ell\nu\ell\nu$ final state.

The leading lepton p_{T} spectrum of the W^+W^- process is sensitive to anomalous gauge boson coupling parameters $\Delta\kappa_\gamma$, $\Delta\kappa_Z$, λ_γ, λ_Z, and Δg_1^Z. Both ATLAS and CMS quote limits in the LEP parametrization [22] that introduces $SU(2) \times U(1)$ gauge invariance constraints to reduce the number of free parameters to Δg_1^Z, $\Delta\kappa_\gamma$, and λ_Z. The obtained limits assuming no form-factor are compared for both expected and

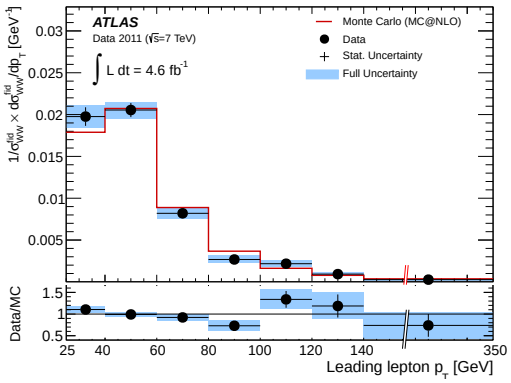

Figure 8. ATLAS measurement of the transverse momentum of the leading lepton in W^+W^- events compared with the SM prediction at $\sqrt{s} = 7$ TeV. The full uncertainty contains statistical and systematic uncertainties.

Table 5. Expected and observed 95% CL limits on the ATGC parameters $\Delta\kappa_\gamma$, λ_Z and Δg_1^Z in the LEP parametrization derived from the leading lepton p_{T} spectrum in W^+W^- production at 7 TeV (ATLAS [8],CMS [11]). No form-factor is applied to the ATGC parameters.

	Observed (CMS)	Observed (ATLAS)	Expected (ATLAS)
Δg_1^Z	$[-0.095, 0.095]$	$[-0.039, 0.052]$	$[-0.039, 0.052]$
$\Delta\kappa_\gamma$	$[-0.21, 0.22]$	$[-0.14, 0.14]$	$[-0.13, 0.13]$
λ_Z	$[-0.048, 0.048]$	$[-0.062, 0.059]$	$[-0.060, 0.059]$

measured 95% CL limits in Table 5.

3.2.4. Semi-leptonic VV production The cross sections for W^+W^- and $W^\pm Z$ production have been measured also in the semileptonic decay channel in the $W^\pm V \to \ell^\pm \nu q\bar{q}$ final state with $V = W^\pm, Z$. The semileptonic final state has a relatively large background mainly from V production with associated jets compared to the fully leptonic decay channels, but offers a substantially larger branching fraction. The increased statistics of signal events at high partonic centre of mass compared to the fully leptonic decay modes enhances specifically the sensitivity to aTGC. ATLAS and CMS have published measurements of the inclusive production cross section $W^+W^- + W^\pm Z$ and set limits on charged aTGC with the full data set of the $\sqrt{s} = 7$ TeV run [9, 12].

Both analysis use the semileptonic decay channel with an electron or muon and two jets in the final state. The event selection sets requirements on the lepton p_{T}, the $E_{\mathrm{T}}^{\mathrm{miss}}$, di-jet invariant mass, and the event topology. The signal fraction of $W^+W^- + W^\pm Z$ in the event sample after selection is only about 1%, and no further selection criteria are applied to distinguish between W^+W^- and $W^\pm Z$ production. The dominant background from $Z/W^\pm$+jets production is constrained with data driven methods, folowed by the sub-leading background contributions from $t\bar{t}$ and multi-jet production. The cross-section is extracted with a simultaneous fit of the di-jet invariant mass spectrum comprising the signal and background components. In Figure 9 the di-jet invariant mass spectrum and the extracted signal after background subtraction from Ref. [9] is shown. The largest systematic uncertainty is related to the modelling of the $Z/W^\pm$+jets background with about 20% on the cross section.

The measured and predicted cross sections are compared in Table 3.2.4.

Experiment	cross section	$\sqrt{s}$	measured	predicted	reference
ATLAS	total	7 GeV	68±7 (stat.) ±19 (syst.+lumi.) pb	61.1 ± 2.2 pb	[9]
CMS	total	7 GeV	68.9 ± ±8.7 (stat.) ±9.7 (syst.) ± 1.5 (lumi.) pb	65.6 ± 2.2 pb	[12]

Table 6. Summary of measured total $W^\pm Z + W^+W^-$ production cross sections from ATLAS and CMS at 7 TeV centre-of-mass energies in the $W^\pm V \to \ell^\pm \nu q\bar{q}$ final state.

To extract limits on aTGC parameters the transverse momentum of the di-jet system $p_{\mathrm{T}}(jj)$ is used by ATLAS and CMS. The resulting 95% CL limits are listed in Table 7. The ATLAS limits use the LEP scenario [22], while the CMS limits are derived in the HISZ [23, 24] scenario. The achieved precision is comparable to the fully leptonic channel.

A measurement of the $W^\pm Z$ and ZZ production cross sections at $\sqrt{s} = 8$ TeV with a data set of 18.9fb^{-1} in the semileptonic final state with two b-quark jets from the $Z$and $\ell^+\ell^-$, $\nu\bar{\nu}$ or $\ell\nu$ has been published by CMS [15], so far the only published results at 8 TeV for these channels. The measured cross sections ($\sigma(pp \to W^\pm Z) = 30.7 \pm 9.3(\mathrm{stat}) \pm 7.1(\mathrm{syst}) \pm 4.1(\mathrm{theo}) \pm 1.0(\mathrm{lumi})$pb and $\sigma(pp \to ZZ) = 6.5 \pm 1.7(\mathrm{stat}) \pm 1.0(\mathrm{syst}) \pm 0.9(\mathrm{theo}) \pm 0.2(\mathrm{lumi})$pb) are consistent with theoretical calculation at NLO in α_s ($\sigma(pp \to ZZ) = 22.3 \pm 1.1$pb and $\sigma(pp \to ZZ) = 7.7 \pm 0.4$pb), with the precision being still statistically limited.

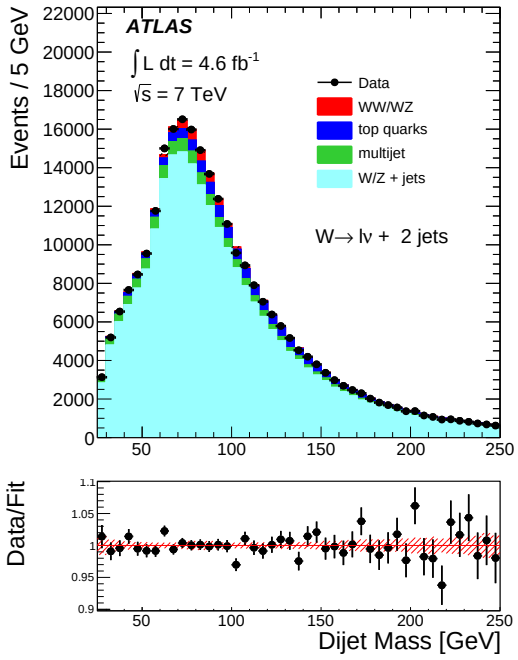

(a)

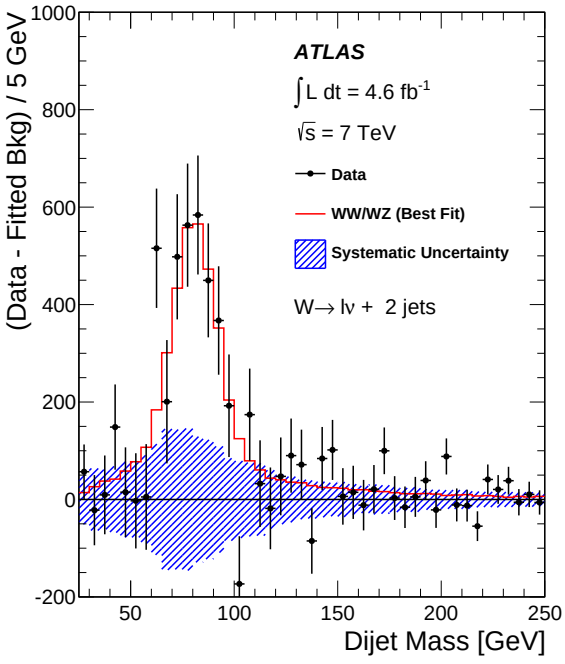

(b)

Figure 9. (a) The di-jet invariant mass spectrum for the sum of electron and muon channels, (b) the distribution of the background subtracted data. The lower panel shows that ratio of data and total fit result.

Table 7. Expected and observed 95% CL on $\Delta\kappa_\gamma$, $\lambda_Z = \lambda_\gamma$ and Δg_1^Zin measured in the $W^\pm V \to \ell^\pm \nu q\bar{q}$ final state from the ATLAS [9] and CMS [12] collaborations.

	CMS	ATLAS	
	Observed	Observed	Expected
$\lambda_Z = \lambda_\gamma$	$[-0.038, 0.030]$	$[-0.039, 0.040]$	$[-0.048, 0.047]$
$\Delta\kappa_\gamma$	$[-0.11, 0.14]$	$[-0.21, 0.22]$	$[-0.23, 0.25]$
Δg_1^Z	–	$[-0.055, 0.071]$	$[-0.072, 0.085]$

ATLAS $W\gamma\gamma$ [25] CMS WVgamma 8 TeV [26]

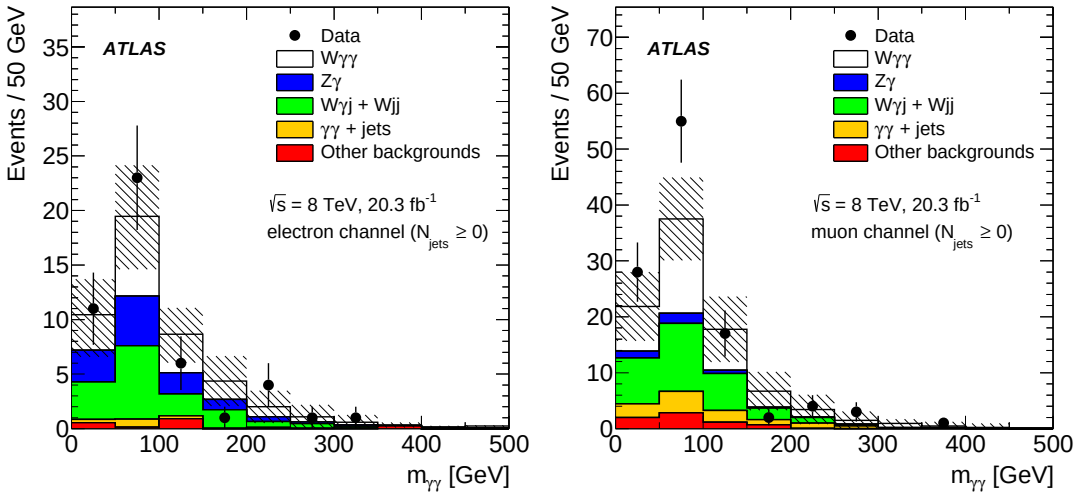

Figure 10.

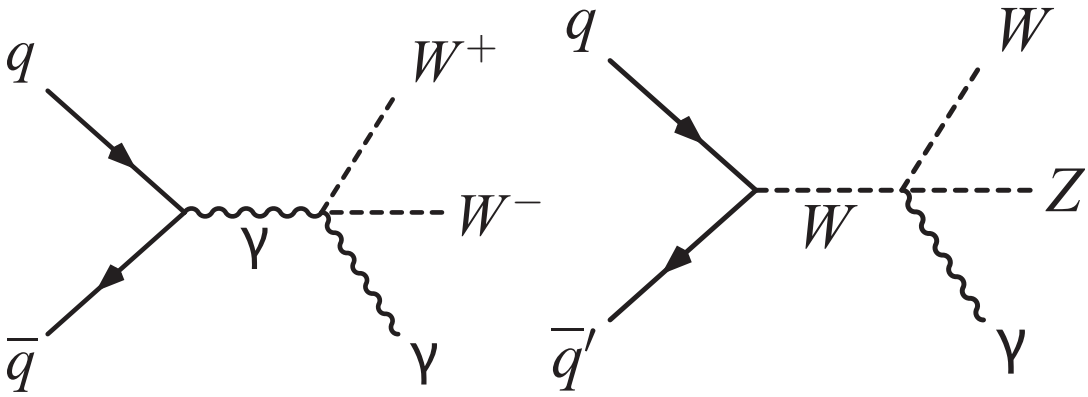

Figure 11.

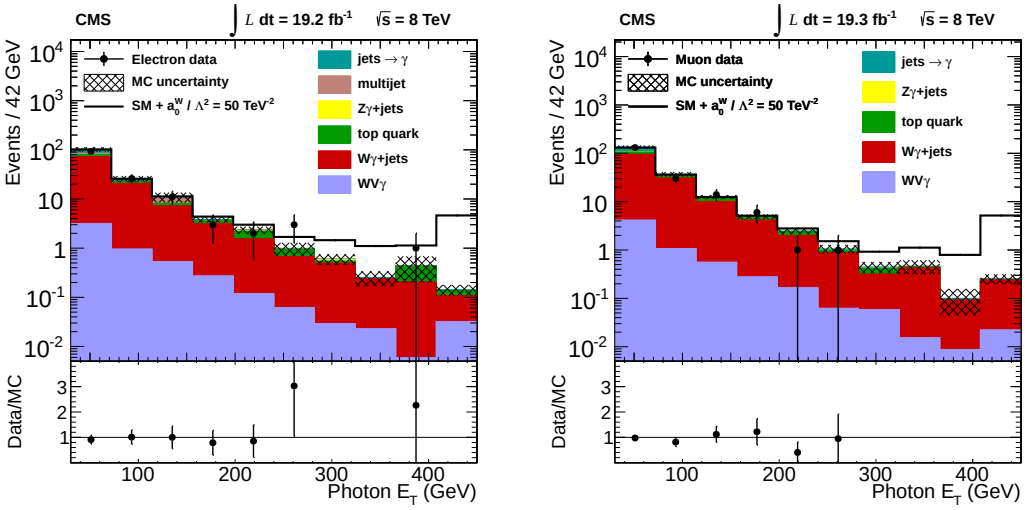

Figure 12.

4. Exclusive boson production

4.1. Exclusive single boson production, vector-boson fusion

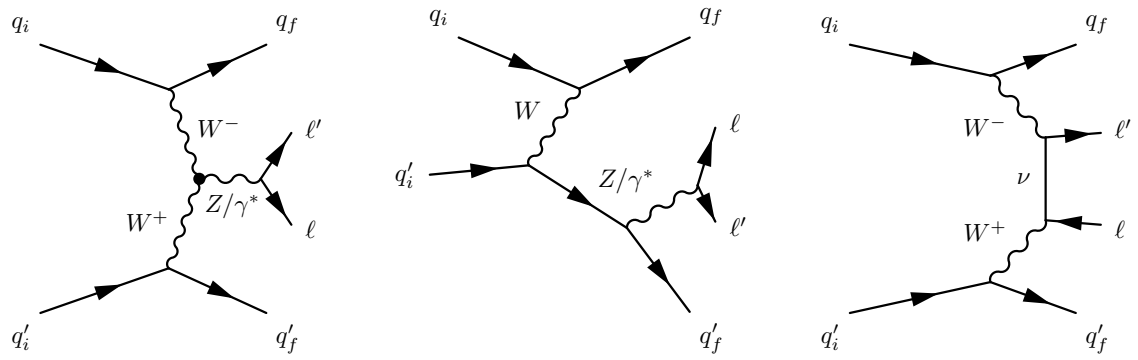

Figure 13. Representative Feynman diagrams for dilepton production in association with two jets from purely electroweak contributions: (left) vector boson fusion, (middle) bremsstrahlung-like, and (right) multiperipheral production.

ATLAS VBF Z 7 TeV [27]
CMS VBF Z 7 TeV [28]
CMS VBF Z 8 TeV [29] Figure 14

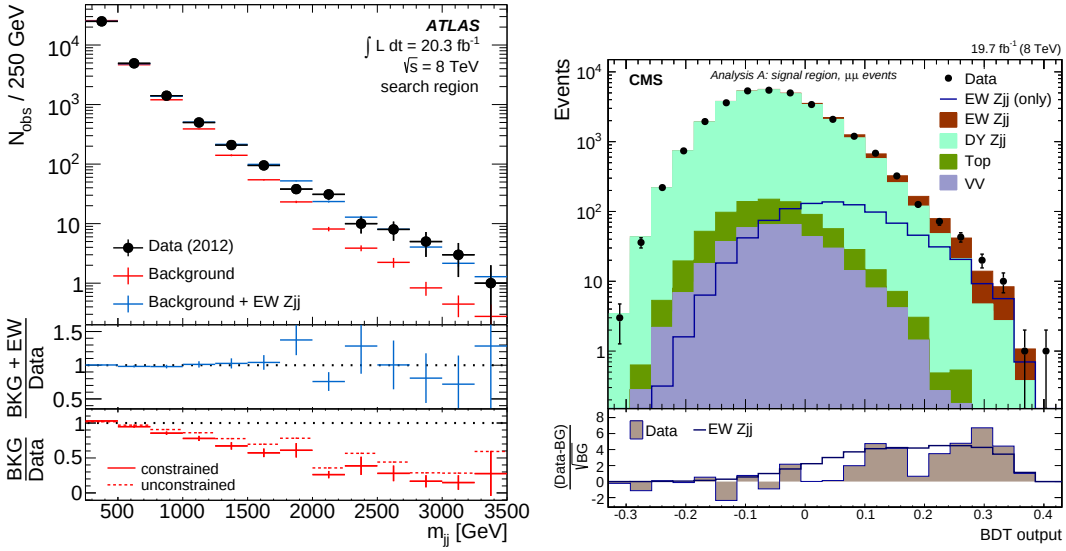

Figure 14. Evidence of observation of an electroweak amplitude in Z+2 jet production. Left: The invariant mass distribution of dijets in Z+2 jet events selected from a signal region by ATLAS. Right: The BDT distribution of Z+2 jet events selected from a signal region by CMS in the dimuon channel.

4.2. Exclusive di-boson production, vector-boson scattering

CMS WWexcl 7 TeV [30] ATLAS SSWW 8 TeV [31] CMS SSWW 8 TeV [32]

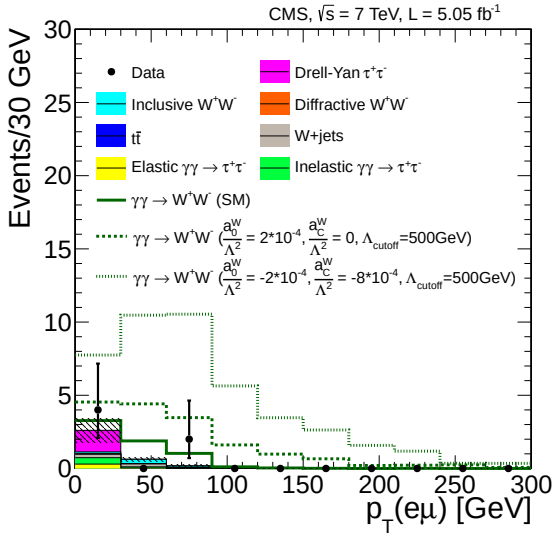

Figure 15.

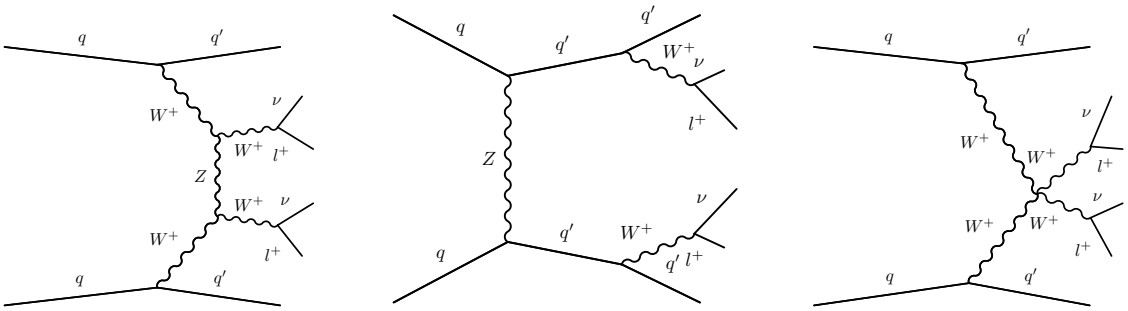

Figure 16. Representative Feynman diagrams for same-sign WW production in association with two jets from purely electroweak contributions: (left) vector boson fusion, (middle) bremsstrahlung-like, and (right) multiperipheral production.

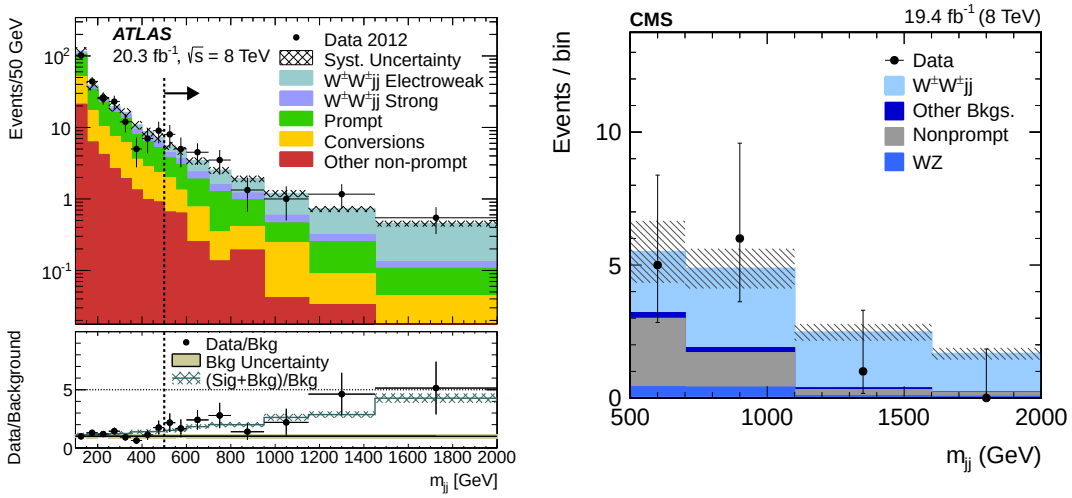

Figure 17. Left: a signal region by ATLAS. Right:

5. Electroweak (precision) tests of the standard model

5.1. Test of tri-boson vertex

ATLAS Wgamma Zgamma 7 TeV [3]
ATLAS WW 7 TeV [8]
ATLAS WW+WZ cross section 7 TeV [9]
ATLAS WZ 7 TeV [14]
ATLAS ZZ4l,ZZ2l2v 7 TeV [16]
CMS ZZ4l 8 TeV [**?**]
CMS ZZ4l 7 TeV [17]
CMS WW2l2n 7 TeV [11]
CMS WWlnjj 7 TeV [12]
CMS WW2l2n 8 TeV(CMS-PAS-SMP-14-016, to be published)
CMS $W^{\pm}\gamma/Z\gamma$ 7 TeV [4]
CMS Znngamma 7 TeV [5]
CMS $Z\gamma$ 8 TeV [6]
CMS $ZZ \to \ell^{\pm}\ell^{-}\nu\bar{\nu}$ 7+8 TeV [18]

5.2. Test of tetra-boson vertex

ATLAS $W\gamma\gamma$ 8 TeV [25]
ATLAS SSWW 8 TeV [31]
CMS WVgamma 8 TeV [26]
CMS WWexcl 7 TeV [30]
CMS SSWW 8 TeV [32]

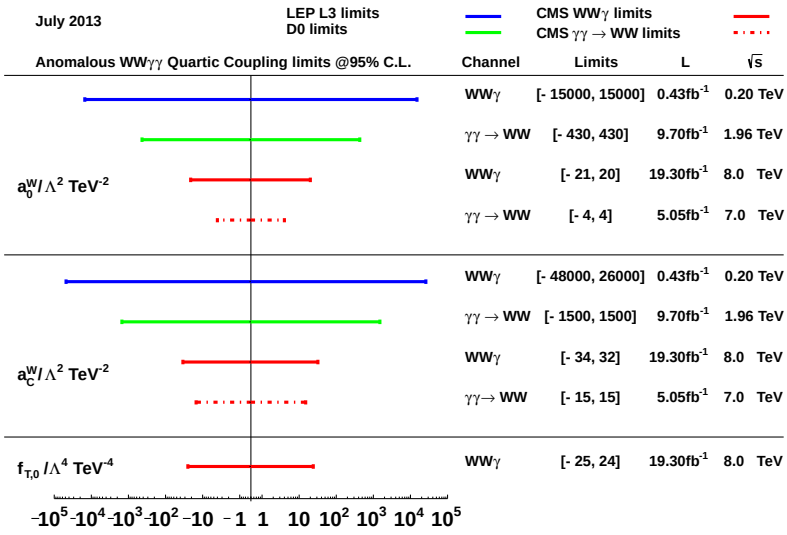
July 2013
LEP L3 limits
D0 limits
CMS WWγ limits
CMS γγ → WW limits
Anomalous WWγγ Quartic Coupling limits @95% C.L.
Channel
Limits
L
√s
WWγ [- 15000, 15000] 0.43fb-1 0.20 TeV
γγ → WW [- 430, 430] 9.70fb-1 1.96 TeV
WWγ [- 21, 20] 19.30fb-1 8.0 TeV
γγ → WW [- 4, 4] 5.05fb-1 7.0 TeV
a0W / Λ2 TeV-2
WWγ [- 48000, 26000] 0.43fb-1 0.20 TeV
γγ → WW [- 1500, 1500] 9.70fb-1 1.96 TeV
WWγ [- 34, 32] 19.30fb-1 8.0 TeV
γγ→ WW [- 15, 15] 5.05fb-1 7.0 TeV
acW / Λ2 TeV-2
fT,0 / Λ4 TeV-4
WWγ [- 25, 24] 19.30fb-1 8.0 TeV
-10^5 -10^4 -10^3 -10^2 -10 -1 1 10 10^2 10^3 10^4 10^5

Figure 18.

5.3. Z AFB and sin thetaW

ATLAS weak mixing angle [33]
CMS weak mixing angle [34]
CMS Drell–Yan AFB 7 TeV [35]
CMS Drell–Yan AFB 8 TeV(CMS-PAS-SMP-14-004, to be published)

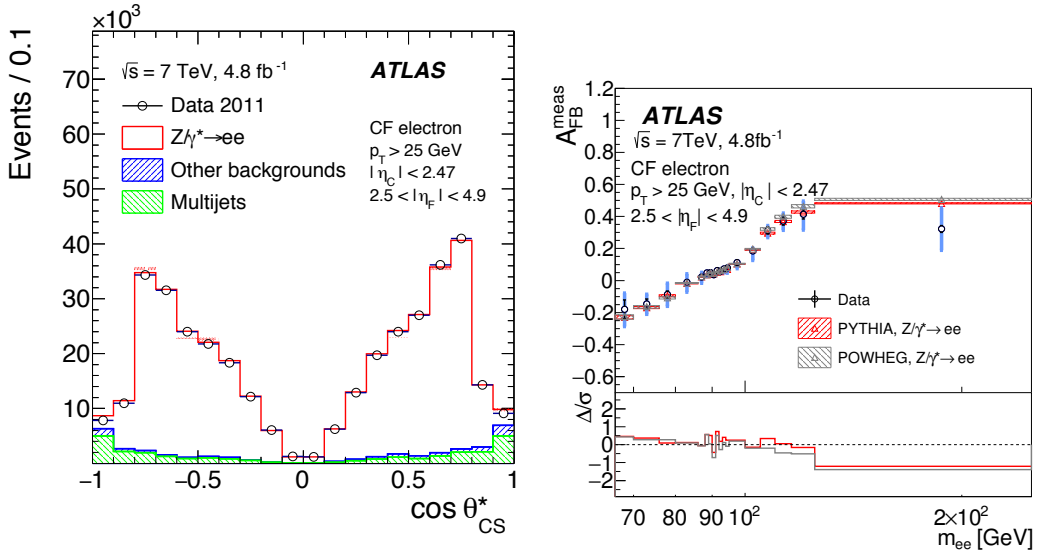

Figure 19. Left: a signal region by ATLAS. Right:

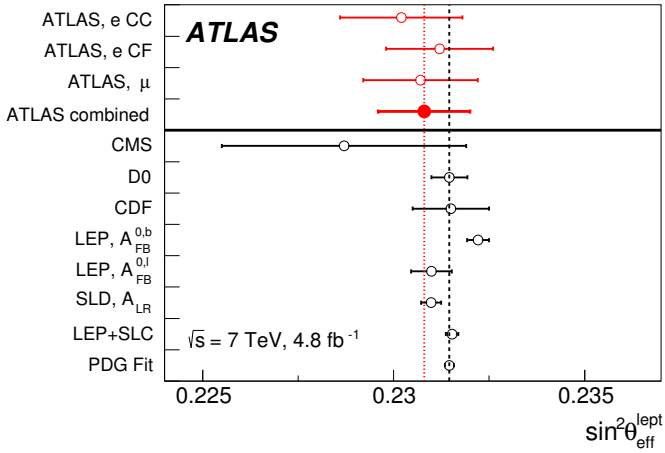

Figure 20.

5.4. W mass

6. Summary

ATLAS [36] CDF [37] CMS [38] D0 [39] LHCb [40]

CDF Z asymmetry muon [41] CDF Z asymmetry electron [42] CDF W mass PRD [43] CDF W mass PRL [44]

D0 W asymmetry electron [45] D0 W asymmetry muon [46] D0 W mass PRD [47] D0 W mass PRL [48]

CDF+D0 W mass combination [49]

Snowmass electroweak [50]

Wmass PDF [51]

Acknowledgments

Acknowledgments go here.

[1] Aad G *et al.* (ATLAS Collaboration) 2013 *Phys.Lett.* **B725** 223–242 (*Preprint* 1305.4192)
[2] Khachatryan V *et al.* (CMS Collaboration) 2015 *Eur.Phys.J.* **C75** 147 (*Preprint* 1412.1115)
[3] Aad G *et al.* (ATLAS Collaboration) 2013 *Phys.Rev.* **D87** 112003 (*Preprint* 1302.1283)
[4] Chatrchyan S *et al.* (CMS Collaboration) 2014 *Phys.Rev.* **D89** 092005 (*Preprint* 1308.6832)
[5] Chatrchyan S *et al.* (CMS Collaboration) 2013 *JHEP* **1310** 164 (*Preprint* 1309.1117)
[6] Khachatryan V *et al.* (CMS Collaboration) 2015 *JHEP* **1504** 164 (*Preprint* 1502.05664)
[7] Aad G *et al.* (ATLAS Collaboration) 2015 *Phys.Rev.* **D91** 052005 (*Preprint* 1407.0573)
[8] Aad G *et al.* (ATLAS Collaboration) 2013 *Phys.Rev.* **D87** 112001 (*Preprint* 1210.2979)
[9] Aad G *et al.* (ATLAS Collaboration) 2015 *JHEP* **1501** 049 (*Preprint* 1410.7238)
[10] 2014 Measurement of the W^+W^- production cross section in proton-proton collisions at $\sqrt{s} = 8$ TeV with the ATLAS detector Tech. Rep. ATLAS-CONF-2014-033 CERN Geneva
[11] Chatrchyan S *et al.* (CMS Collaboration) 2013 *Eur.Phys.J.* **C73** 2610 (*Preprint* 1306.1126)
[12] Chatrchyan S *et al.* (CMS Collaboration) 2013 *Eur.Phys.J.* **C73** 2283 (*Preprint* 1210.7544)
[13] Chatrchyan S *et al.* (CMS Collaboration) 2013 *Phys.Lett.* **B721** 190–211 (*Preprint* 1301.4698)
[14] Aad G *et al.* (ATLAS Collaboration) 2012 *Eur.Phys.J.* **C72** 2173 (*Preprint* 1208.1390)
[15] Chatrchyan S *et al.* (CMS Collaboration) 2014 *Eur.Phys.J.* **C74** 2973 (*Preprint* 1403.3047)
[16] Aad G *et al.* (ATLAS Collaboration) 2013 *JHEP* **1303** 128 (*Preprint* 1211.6096)
[17] Chatrchyan S *et al.* (CMS Collaboration) 2013 *JHEP* **1301** 063 (*Preprint* 1211.4890)
[18] Khachatryan V *et al.* (CMS Collaboration) 2015 (*Preprint* 1503.05467)
[19] Khachatryan V *et al.* (CMS) 2015 *Phys. Lett.* **B740** 250–272 (*Preprint* 1406.0113)
[20] Herndon M 2015 Limits on anomalous triple and quartic gauge couplings URL https://twiki.cern.ch/twiki/bin/view/CMSPublic/PhysicsResultsSMPaTGC
[21] LEP Electroweak Gauge-Couplings Group 2002 A combination of preliminary results on gauge boson couplings measured by the lep experiments URL http://lepewwg.web.cern.ch/lepww/tgc/summer02
[22] Gounaris G *et al.* 1996 Triple gauge boson couplings *AGS / RHIC Users Annual Meeting Upton, New York, June 15-16, 1995* (*Preprint* hep-ph/9601233) URL http://alice.cern.ch/format/showfull?sysnb=0215385
[23] Hagiwara K, Ishihara S, Szalapski R and Zeppenfeld D 1992 *Physics Letters B* **283** 353 – 359 ISSN 0370-2693 URL http://www.sciencedirect.com/science/article/pii/037026939290031X
[24] Hagiwara K, Ishihara S, Szalapski R and Zeppenfeld D 1993 *Phys. Rev. D* **48**(5) 2182–2203 URL http://link.aps.org/doi/10.1103/PhysRevD.48.2182
[25] Aad G *et al.* (ATLAS Collaboration) 2015 (*Preprint* 1503.03243)

[26] Chatrchyan S *et al.* (CMS Collaboration) 2014 (*Preprint* 1404.4619)
[27] Aad G *et al.* (ATLAS Collaboration) 2014 *JHEP* **1404** 031 (*Preprint* 1401.7610)
[28] Chatrchyan S *et al.* (CMS Collaboration) 2013 *JHEP* **1310** 062 (*Preprint* 1305.7389)
[29] Khachatryan V *et al.* (CMS Collaboration) 2015 *Eur.Phys.J.* **C75** 66 (*Preprint* 1410.3153)
[30] Chatrchyan S *et al.* (CMS Collaboration) 2013 *JHEP* **1307** 116 (*Preprint* 1305.5596)
[31] Aad G *et al.* (ATLAS Collaboration) 2014 *Phys.Rev.Lett.* **113** 141803 (*Preprint* 1405.6241)
[32] Khachatryan V *et al.* (CMS Collaboration) 2015 *Phys.Rev.Lett.* **114** 051801 (*Preprint* 1410.6315)
[33] Aad G *et al.* (ATLAS Collaboration) 2015 (*Preprint* 1503.03709)
[34] Chatrchyan S *et al.* (CMS Collaboration) 2011 *Phys.Rev.* **D84** 112002 (*Preprint* 1110.2682)
[35] Chatrchyan S *et al.* (CMS Collaboration) 2013 *Phys.Lett.* **B718** 752–772 (*Preprint* 1207.3973)
[36] Aad G *et al.* (ATLAS Collaboration) 2008 *JINST* **3** S08003
[37] Abulencia A *et al.* (CDF Collaboration) 2007 *J.Phys.* **G34** 2457–2544 (*Preprint* hep-ex/0508029)
[38] Chatrchyan S *et al.* (CMS Collaboration) 2008 *JINST* **3** S08004
[39] Abazov V *et al.* (D0 Collaboration) 2006 *Nucl.Instrum.Meth.* **A565** 463–537 (*Preprint* physics/0507191)
[40] Alves A Augusto J *et al.* (LHCb Collaboration) 2008 *JINST* **3** S08005
[41] Aaltonen T A *et al.* (CDF Collaboration) 2014 *Phys.Rev.* **D89** 072005 (*Preprint* 1402.2239)
[42] Aaltonen T *et al.* (CDF Collaboration) 2013 *Phys.Rev.* **D88** 072002 (*Preprint* 1307.0770)
[43] Aaltonen T A *et al.* (CDF Collaboration) 2014 *Phys.Rev.* **D89** 072003 (*Preprint* 1311.0894)
[44] Aaltonen T *et al.* (CDF Collaboration) 2012 *Phys.Rev.Lett.* **108** 151803 (*Preprint* 1203.0275)
[45] Abazov V M *et al.* (D0 Collaboration) 2014 *Phys.Rev.Lett.* **112** 151803 (*Preprint* 1312.2895)
[46] Abazov V M *et al.* (D0 Collaboration) 2013 *Phys.Rev.* **D88** 091102 (*Preprint* 1309.2591)
[47] Abazov V M *et al.* (D0 Collaboration) 2014 *Phys.Rev.* **D89** 012005 (*Preprint* 1310.8628)
[48] Abazov V M *et al.* (D0 Collaboration) 2012 *Phys.Rev.Lett.* **108** 151804 (*Preprint* 1203.0293)
[49] Aaltonen T A *et al.* (CDF Collaboration, D0 Collaboration) 2013 *Phys.Rev.* **D88** 052018 (*Preprint* 1307.7627)
[50] Baak M, Blondel A, Bodek A, Caputo R, Corbett T *et al.* 2013 (*Preprint* 1310.6708)
[51] Bozzi G, Rojo J and Vicini A 2011 *Phys.Rev.* **D83** 113008 (*Preprint* 1104.2056)